Article:

Al-musawi, H., Figueiredo, F.P., Guadagnini, M. orcid.org/0000-0003-2551-2187 et al. (1 more author) (2019) Shrinkage properties of plain and recycled steel–fibre-reinforced rapid hardening mortars for repairs. Construction and Building Materials, 197. pp. 369-384. ISSN 0950-0618

https://doi.org/10.1016/j.conbuildmat.2018.11.099

Shrinkage properties of plain and recycled steel–fibre-reinforced rapid hardening mortars for repairs

Hajir Al-musawi [a,*], Fabio P. Figueiredo [a], Maurizio Guadagnini [a], Kypros Pilakoutas [a]

[a]*Department of Civil and Structural Engineering, The University of Sheffield, Sir Frederick Mappin Building, Mappin Street, S1 3JD Sheffield, UK.*

* Corresponding author's email: Haal-musawi1@sheffield.ac.uk Tel: +44 (0) 114 222 5729, Fax: +44 (0) 114 2225700

HIGHLIGHTS

- Non-uniform drying of rapid hardening overlays can lead to cracking and delamination.
- Mixes with CSA cement showed much lower shrinkage strains than mixes with RSC cement.
- RSC and FRSC mixes showed considerable autogenous shrinkage at the age of 60 days.
- FE analysis were used to predict shrinkage development using hygral contraction coefficient.
- Creep plays an important role in moderating stresses of overlays.

Abstract

This article investigates the time dependent transport properties and shrinkage performance of rapid hardening plain and fibre reinforced mortars for repair applications. Two plain and two SFRC mixes with 45 kg/m^3 of recycled clean steel fibers made with rapid hardening cements (CSA - calcium sulfoaluminate cement and RSC - calcium aluminate cement) are studied. It is found that mixes with CSA cement have much lower shrinkage values (around 220 and 365 microstrains) compared to mixes with RSC cement (around 2690 and 2530 microstrains), but most of the shrinkage in these mixes is autogenous. Nonetheless, fibres reduce the drying shrinkage of RSC cement mixes by approximately 12%. Model code 2010 and ACI equations can be used to estimate the shrinkage development with

time for these mixes provided suitable parameters for each cement type are adopted. Inverse analysis using finite element method is successfully employed to determine the moisture diffusivity and the hygral contraction coefficient of each mix. A comparison is made between the values of shrinkage strain predicted by the numerical models over time, for different depths, and code equations. A simple analytical procedure is used to assess cracking and/or delamination risks due to restrained shrinkage for these materials in overlay applications.

Key words*:* SFRC, rapid hardening cements, shrinkage and transport properties, FE analysis

1. Introduction

Concrete overlays are extensively used in the repair and strengthening of concrete structures either to replace damaged concrete or directly cast as a new layer. In both applications, moisture from the fresh layer does not only diffuse to the environment, but also to the concrete substrate, resulting in faster drying shrinkage. Shrinkage is restrained by the substrate layer leading to tensile and interfacial shear stresses in the repair layer. These stresses, if they exceed material capacity, can lead to cracking and/or debonding, accelerating the deterioration of the repairs [1]. The cracking potential of repairs increases in rapid hardening materials that are often used to minimise disruption during repair works, due to faster shrinkage rate [2] and lower creep compliance [3].

Although fibres are reported to have a marginal effect in preventing shrinkage strains from developing in concrete, they are used to control crack widths [4] as well as increase tensile strength and fatigue resistance [5] in an attempt to achieve more durable repair layers. To reduce the environmental impact of manufactured steel fibres (MSF), recycled clean steel fibres can also be used as alternative fibre reinforcement [6, 7].

Recycled clean steel fibres (RCSF) were obtained by recycling steel fibre cords, left over from the manufacture of tyres. As a result, they have a consistent length as opposed to recycled tyre steel fibres

(RTSF) which are extracted mechanically from post-consumer tyres and, thus, have more variable lengths.

Since crack width is one of the main parameters that governs the durability of repairs [8], a thorough understanding of the effect of moisture movement and restraint from the substrate is needed to predict crack development in concrete, a material which has widely varied and dynamic porosity systems [9]. The moisture transport mechanism of cementitious mixes is complex and is the subject of extensive research [9-17]. FRC mixes, however, have been studied to a lesser extent [15, 18]. It is known that w/c ratio, cement content and cement type, directly affect moisture diffusion. Fibres may also affect the moisture transport properties of concrete by changing the porosity structure and thus their effect needs to be better understood.

Silfwerbrand [19] provided an analytical procedure to calculate the tensile and shear stresses that develop in overlaid concrete layers and determine the risk of cracking and/or delamination. However, this procedure does not calculate cracking widths, a vital aspect in predicting concrete performance. Eurocode 2 (EC) [20], Model Code 2010 (MC) [21] and ACI 209.2R-08 (ACI) [22] provide procedures to predict shrinkage strain evolution for concrete structures of certain cement types with good accuracy. However, they do not account for rapid hardening cements for which often little information is provided by manufacturers other than setting time and strength. They also do not consider the effect of fibres on concrete shrinkage strain in the predictive equations.

This paper presents a detailed investigation on the time dependent transport properties and shrinkage performance of rapid hardening plain and fibre reinforced mortars for repair applications. It starts by reviewing the factors involved in diffusion and shrinkage of both plain and FRC mixes. It then presents experimental work on moisture movement and shrinkage. The results are used in inverse analysis to determine the moisture diffusion coefficient, surface factor and shrinkage hygral coefficient which are needed to predict shrinkage performance. The available code procedures to predict the shrinkage of these mixes over time are also evaluated and new factors for each cement type are proposed. The Silfwerbrand procedure is then used to determine cracking and delamination risks.

2. Moisture diffusion and shrinkage

Moisture movement during drying of concrete is characterised by two stages; a constant drying rate stage which is succeeded by a falling drying rate [12, 15, 23], depending on the degree of continuity between liquid and vapour phases and on driving force variations [16]. At the beginning of drying, the evaporation rate is constant and is approximately equal to the rate of evaporation of water exposed to the same conditions [24-25]. As the cementitious material is fully saturated, there is no hydraulic potential gradient to drive the moisture movement inside the porous medium and the internal vapour pressure is equivalent to the saturated vapour pressure. However, at the boundary layer, there is a pressure variation from saturated vapour pressure to ambient vapour pressure, driving moisture out to the surrounding air. Moisture evaporation at the surface causes a slight reduction in vapour pressure [16]. This small vapour pressure gradient is sufficient to cause moisture flow towards the surface, since at this stage the hydraulic diffusivity is high [26]. As drying continues, moisture decreases inside the material. Drying is still considered to be in stage one as long as the capillary system is saturated. When the liquid phase becomes discontinuous upon further drying, a transition from stage one to stage two takes place, at which diffusion of water vapour becomes the dominant mechanism for moisture transport [26]. During this stage, the evaporation rate drops, as moisture is only limited to movement of water vapour rather than liquid water diffusion [27] as is the case in the first stage, and the vapour pressure falls below the saturation vapour pressure value. The moisture content continues to decrease until vapour pressure reaches ambient level. Figure 1 shows a typical cumulative moisture loss and evaporation rate during stage one and stage two for a cement paste sample [15]. It is shown that during stage one, the drying behaviour is independent of capillary microstructure [26]. In a study performed by Bakhashi & Mobasher [15] to investigate the effect of curing time on the diffusion characteristics of cement paste, it was found that the moisture loss was substantially reduced by curing the cement paste for 24 hours and the transition from stage one to stage two took place quicker compared to non-cured samples. This can be attributed to microstructural and pore distribution changes with additional hydration. It can be argued that for fast setting materials, stage one is expected to be much shorter than for conventional mortar, as most hydration takes place during the first few hours and phase transition happens faster. This will be investigated in this paper to understand the role of cement type on diffusion properties.

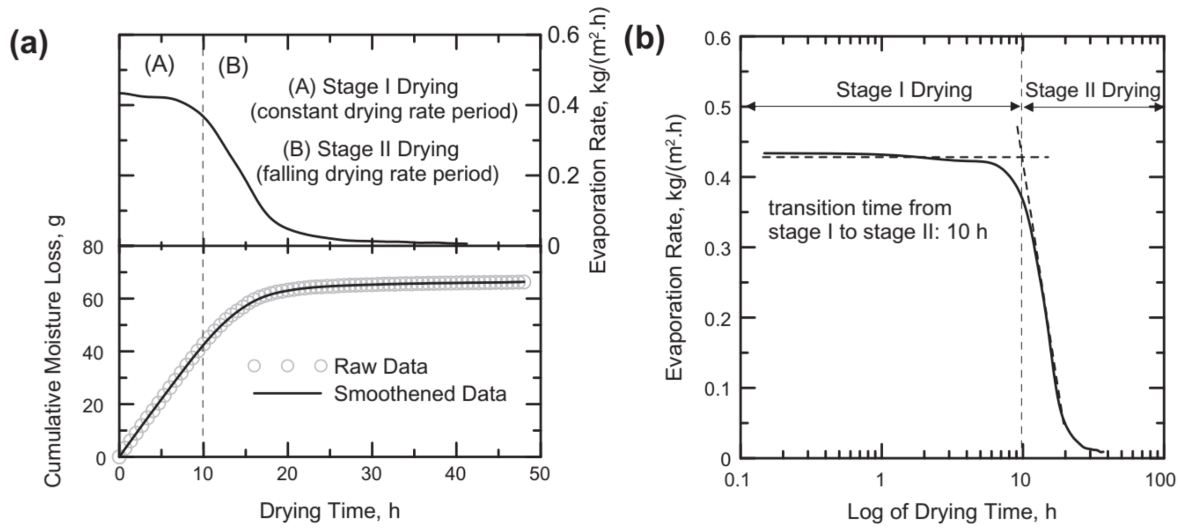

Figure 1. Typical cumulative moisture loss and evaporation rate of a cement paste sample versus time: (a) in linear scale; (b) in log scale [15]

Fick's second law (Equation **1**) can be used to model moisture movement in concrete for various stages of drying, with a moisture diffusivity that represents liquid and vapour diffusion [16].

$$\frac{\partial C}{\partial t} = D\frac{\partial^2 C}{\partial X^2}$$ Equation **1**

where C is the moisture concentration (kg/m^3), D is the moisture diffusion coefficient (m^2/s) and t is time (s).

As the moisture transfer equations are analogous to heat transfer equations and heat transfer analysis is readily available in FEA packages, this analogy is often exploited for moisture transfer studies [16, 18, 28].

Another important factor in moisture distribution problems is the surface factor or convective factor (ƒ). This factor determines the moisture exchange between the concrete surface and the atmosphere. It depends on several other factors like the w/c ratio [11] and wind speed [29]. A wide range of surface factors is reported in literature [(0.75-7.5 mm/day [11]), 18, 29]. However, this parameter can be determined by inverse analysis for specific mortar mixes to improve the accuracy of the predicted moisture distribution.

The hydro-shrinkage coefficient (also called hygral contraction coefficient) is a factor that links free shrinkage strain to moisture content. It is a unique material property for each mix type. An exponential relationship was found by Ayano and Wittmann [13] while Huang et al. [28] used a linear relationship to simulate non-linear shrinkage in box girders. This factor can also be obtained through inverse analysis.

3. Experimental program

3.1. Mix proportions

Two plain and two SFRC mixes with 45 kg/m^3 (V_f = 0.57%) of recycled clean steel fibres (RCSF) were investigated in this study, details of which are given in Table 1. Two commercial cement types were used: calcium sulfoaluminate cement (CSA); and rapid setting calcium aluminate cement (RSC). River washed sand (0-5mm, SG=2.65) was used as fine aggregates. The length of the RCSF used in this study is 21 mm and the diameter is 0.2 mm. Further details on the mixes and material characteristics are given elsewhere [6].

Table 1

Mix proportions

Mix	Cement (kg/m^3)	w/c	SP[a]	Sand (kg/m^3)	Fibre dosage (kg/m^3)
CSA	600	0.40	0.6	1420	0
FCSA	600	0.41	0.61	1420	45
RSC	600	0.35	0.2	1300	0
FRSC	600	0.36	0.21	1300	45

[a] % by cement mass.

3.2. Flexural and Compressive strength

To characterize the flexural performance, mortar prisms of 40*40*160 mm were tested according to BS EN 13892-2, (2002) [30] in displacement control to better capture the post-peak behaviour. A specially designed aluminum yoke (based on the Japanese standard JSCE-SF4 [31]) was mounted on the specimens. The prisms were tested at different ages ranging from one hour up to one year to assess the flexural behaviour over time. After flexural testing, the two parts of the fractured prisms were tested under uniaxial compressive loading according to BS EN 13892-2, (2002) [30]. The results in terms of first cracking strength ($f_{ctm,fl}$) and compressive strength (f_{cu}) (associated standard deviation is given in brackets) are shown in Table 2.

Table 2

Flexural strength ($f_{ctm,fl}$) and compressive strength (f_{cu}) for all mixes (MPa)

Time (Days)	FCSA		FRSC		CSA		RSC	
	$f_{ctm,fl}$	f_{cu}	$f_{ctm,fl}$	f_{cu}	$f_{ctm,fl}$	f_{cu}	$f_{ctm,fl}$	f_{cu}
(1hr) 0.0417	3.52	26.13 (4.61)	3.52	21.34 (3.04)	2.58	21.14 (2.96)	2.53	17.23 (1.92)
(3hrs) 0.125	6.76	31.55 (3.69)	3.54	28.29 (3.54)	3.98	26.92 (2.78)	2.86	24.16 (2.04)
1	6.46	36.60 (2.27)	4.98	37.92 (2.40)	4.34	31.75 (2.51)	3.54	33.01 (2.00)
7	8.18	41.05 (3.27)	5.54	46.16 (3.20)	5.30	35.97 (3.02)	4.22	40.38 (2.43)
28	8.67	43.13 (3.23)	5.65	51.52 (2.88)	5.37	38.62 (2.30)	4.39	46.51 (2.61)
365	8.67	45.47 (3.03)	5.63	54.49 (6.64)	5.40	40.90 (2.27)	4.48	48.09 (3.74)

3.3. Moisture measurement in mortars

To obtain the time history of the moisture profile, needed to obtain the moisture diffusivity of the repair layers, the modified gravimetric method was adopted following the approach of Jafarifar [18]. It involves casting all specimens at the same height and then cutting them at different depths before putting them back together. Thus, the boundary condition from the underlying depth of the concrete specimens is preserved by keeping both segments in contact for the duration of the measurements.

The specimens were cast in 200*50*50 mm steel moulds. After around the expected setting time, water was added to the samples, while still in the moulds and they were covered with plastic sheets to prevent moisture evaporation. The setting time of cement pastes was assessed by the authors [6] using an automatic Vicat apparatus according to ASTM C191 (2013) [32]. The final setting time for CSA, FCSA, RSC and FRSC were 10.5, 11, 14.5 and 15 minutes. After around 40 minutes of curing, the samples were demoulded. Each prism was then immediately sliced into two segments at the prescribed depths of 10, 20, 30 mm, under wet conditions. Their weights were recorded, and the specimens were directly wrapped with cling film and sealed using a high performance ply laminated plastic foil tape. The surfaces 1-5 for the bottom segment and 1-4 for the upper part of the sliced specimens were sealed separately [Figure 2], creating one dimensional drying conditions.

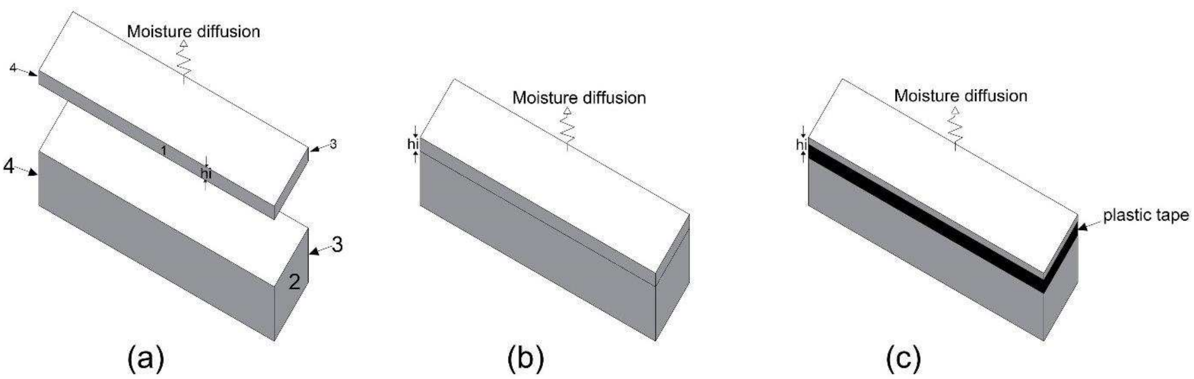

Figure 2. Sealing specimens for the modified gravimetric method

After each weight measurement, the two segments were assembled back together [Figure 2] and the joint was sealed using a new plastic tape [Figure 2]. The weight measurements were taken at one hour and a half, three hours, one day and every day for one week. They were then recorded every week for one month and monthly for four months. After four months, the specimens were unwrapped and dried in the oven for ten days at 70 C^0. After that, the two parts of each prism were weighed. The details of how to determine the moisture content at each depth over time is given in [11,18].

3.4 Free shrinkage measurement

The ASTM C157/C157M (2008) standard [33] for measuring shrinkage of mortars adopts prisms of dimension of 25*25*285 mm. However, due to the use of fibres with a length of 21 mm and to minimize the boundary effects, it was decided to use bigger prisms of 40*40*160 mm instead. As for the specimens used for moisture transport studies, the specimens were cured for around 40 minutes in the moulds. After the curing, the specimens were demolded and demec points were attached to them. The total number of shrinkage samples for each mix was six prisms. Three prisms were kept in an environmental chamber with a relative humidity of 40±3% and temperature of 21±2 C^0 to measure the total shrinkage while the other three prisms were wrapped in cling film and left in a mist room to measure their autogenous shrinkage. After that, they were only unwrapped to take measurements. Shrinkage was measured on both faces of each prism using a 100 mm Demec gauge. The shrinkage measurements started at one hour and a half and continued at frequent time intervals up to 120 days.

4. Experimental results and discussion

4.1. Moisture measurements

The time history of moisture content for each mix is shown in Figure 3. Each curve represents the mean value of two samples. The results confirm that drying is non-uniform across the depth of the specimens with faster drying at the top. For all the mixes, the water content of the upper layer ranges between 0.59 – 0.62 compared with 0.67 – 0.78 for the lower layers.

At the beginning of drying, the rate of drying is relatively faster for RSC and FRSC mixes compared to specimens with CSA and FCSA mixes. However, the rate of drying slows down towards the end of the drying period. The experimental moisture profiles are used in the following section to back calculate moisture diffusivity and surface factor for each mix.

Although literature states that fibre may affect the moisture transport properties of concrete, in this article, however, the fibre inclusion was confirmed not to have a major role on the moisture transport properties of rapid hardening mortar mixes, which allows the use of the MC equation [21], that is usually used to estimate the moisture diffusivity of plain concrete, to calculate their moisture diffusivities.

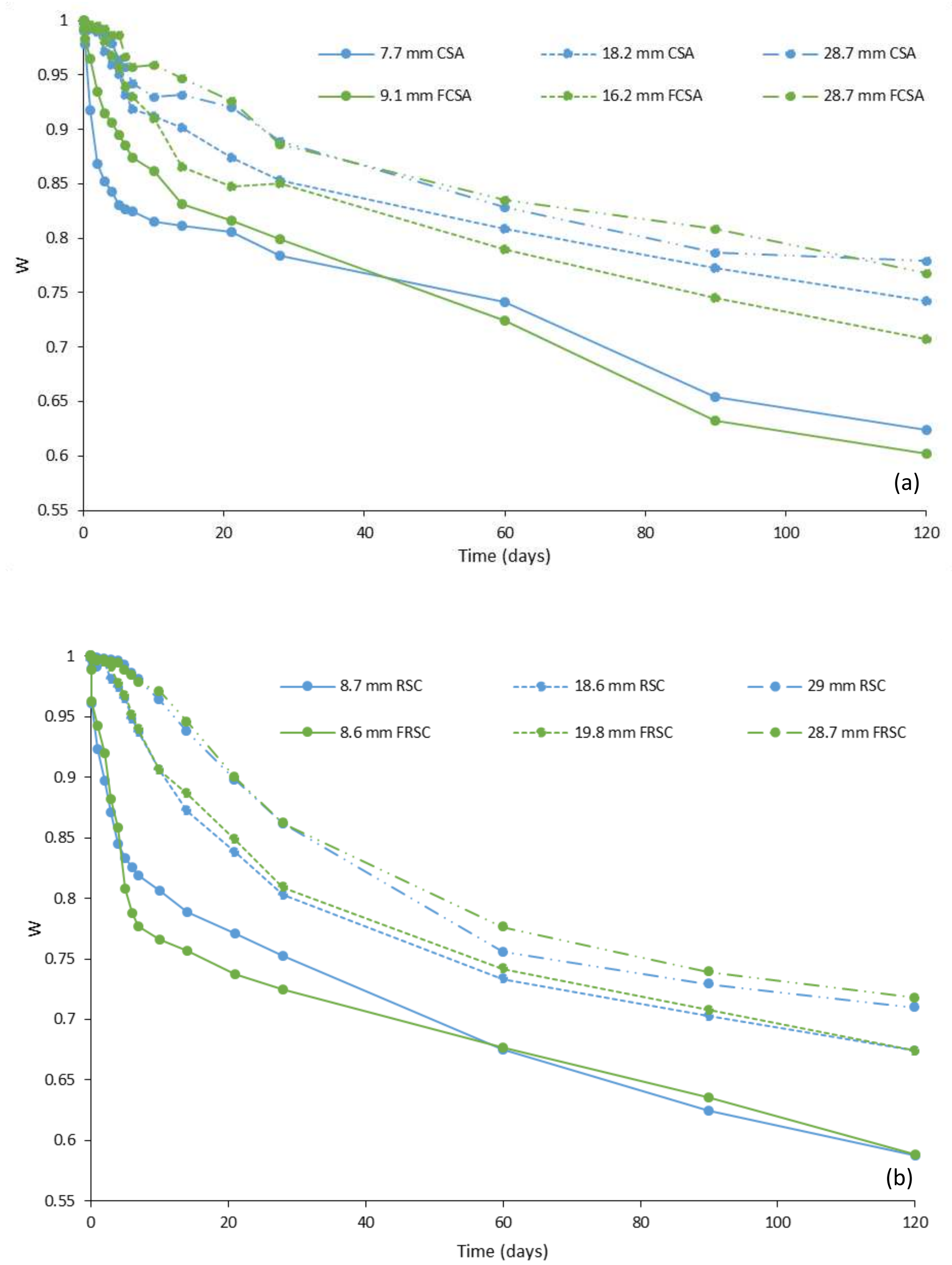

Figure 3. Experimental moisture profiles: (a) CSA and FCSA mixes; (b) RSC and FRSC mixes

4.2. Free shrinkage results

The shrinkage evolution with time for all mixes is shown in Figure 4. Although a direct comparison between the shrinkage of CSA and RSC mixes is not possible due to differences in w/c ratio, superplasticizer dosage and aggregate content, the substantial difference in their shrinkage values can mainly be attributed to the different cement types. As expected, mixes with CSA cement showed much lower shrinkage strains than mixes with RSC cement. This is due to the expansive nature of their hydration products [34] and their higher water consumption during hydration [35]. For RSC cement, the reaction of its main component, monocalcium aluminate (CA), with water results in CAH_{10} and C_2AH_8 as the main hydration products as in Equation **2** and Equation **3** [36]:

$$CA + 10H \rightarrow CAH_{10} \qquad \text{Equation } \mathbf{2}$$

$$2CA + 16H \rightarrow C_2AH_8 + AH_3 \qquad \text{Equation } \mathbf{3}$$

The subsequent conversion reactions of the metastable phases to the stable phases are:

$$2\mathrm{CAH}_{10} \rightarrow \mathrm{C_2AH_8} + \mathrm{AH_3} + 9\mathrm{H} \qquad \text{Equation } \mathbf{4}$$

$$3\mathrm{C_2AH_8} \rightarrow 2\mathrm{C_3AH_6} + \mathrm{AH_3} + 9\mathrm{H} \qquad \text{Equation } \mathbf{5}$$

While for CSA cement, the main crystalline hydration products (ettringite and monosulfate) require more water to form as per Equation **6** and Equation **7** [35]:

$$\mathrm{C_4A_3S} + 18\mathrm{H} \rightarrow \mathrm{C_3A.CS.12H} + 2\mathrm{AH_3} \qquad \text{Equation } \mathbf{6} \qquad \text{(monosulfate formation)}$$

$$\mathrm{C_4A_3S} + 2\mathrm{CSH_2} + 34\mathrm{H} \rightarrow \mathrm{C_3A.3CS.32H} + 2\mathrm{AH_3} \qquad \text{Equation } \mathbf{7} \qquad \text{(ettringite formation)}$$

If less free water is available for drying, then less drying shrinkage can occur.

FCSA develops higher shrinkage strains compared to CSA at all ages. It is known that fibre inclusion introduces air in the mix [18, 37]. Also, the water content and SP dosage are higher for FCSA compared to CSA mix which can contribute to the higher recorded shrinkage values.

The provisions of EC, MC and ACI code were followed to obtain the shrinkage development of CSA and FCSA mixes with time. Both EC and MC require defining parameters αds_1 and αds_2 which depend on cement type. For the cements used, these parameters were obtained by nonlinear regression analysis. The ACI requires defining the ultimate shrinkage strain ε_{shu}. This value was obtained by multiplying the cumulative product of the correction parameters (γ_{sh}, as defined in [22]) by a factor P, obtained by non-linear regression analysis. The predicted and experimental free shrinkage strain for CSA and FCSA are given in Figure 5. As shown, the codes can predict the shrinkage evolution of these mixes reasonably well provided suitable parameters for cement type are used.

The autogenous shrinkage strains obtained for both CSA and FCSA sealed specimens were very small which indicates that some expansive reactions took place and, hence, not shown in Figure 4. On the other hand, both RSC and FRSC mixes showed considerable autogenous shrinkage, 1644 με and 1722 με at the age of 60 days respectively, which accounts for about 64 % and 71% of their total shrinkage at this age, respectively. Mixes with RSC cement has higher compressive strength compared to CSA cement mixes. Autogenous shrinkage is known to be directly related to compressive strength. In addition to, RSC has higher cement fineness that can increase the shrinkage [38]. High autogenous shrinkage can also be attributed to conversion of RSC cement. Nevertheless, no compressive strength reduction was noticed for RSC and FRSC specimens stored in the same conditions [6].

By examining further the RSC and FRSC results, it can be seen that drying shrinkage cannot be obtained by simply deducting autogenous shrinkage from the total shrinkage as the autogenous shrinkage continues at a faster rate than drying, possibly because drying affects the nature of the hydration reactions [39]. Thus, an alternative method is needed to derive the drying shrinkage. MC relates the autogenous shrinkage (shr_{Auto}) to the compressive strength at 28 days and to the type of cement.

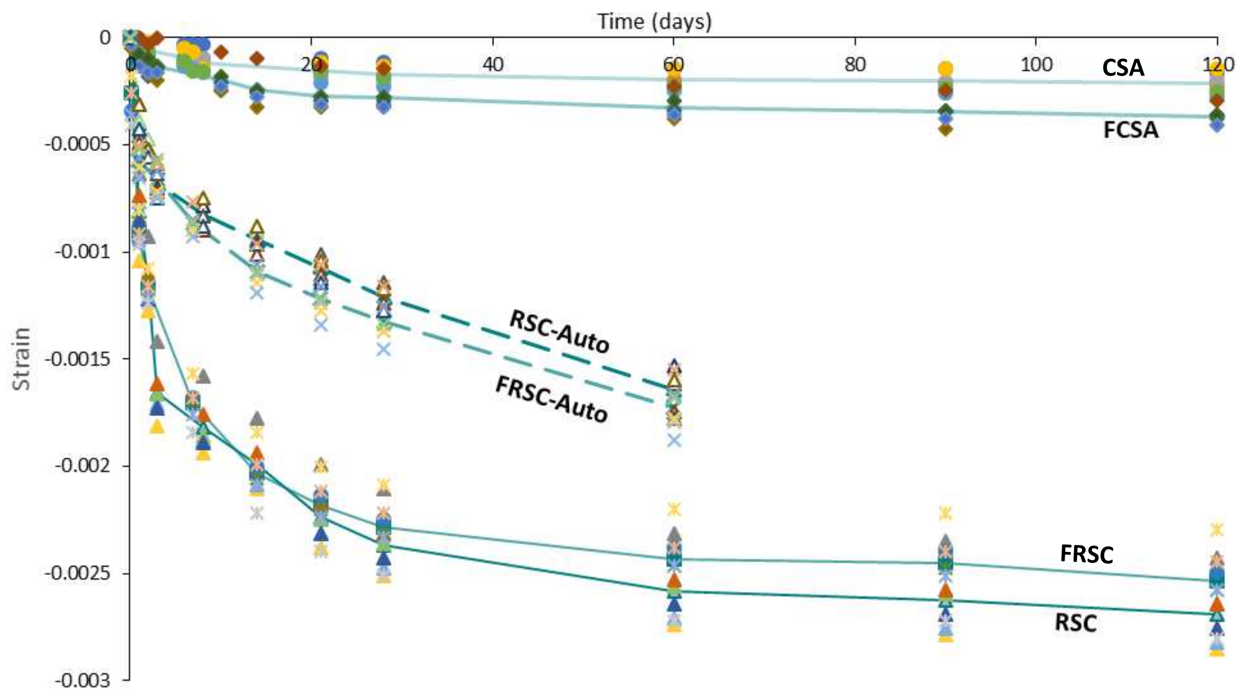

Figure 4. Experimental shrinkage development for all mixes with time

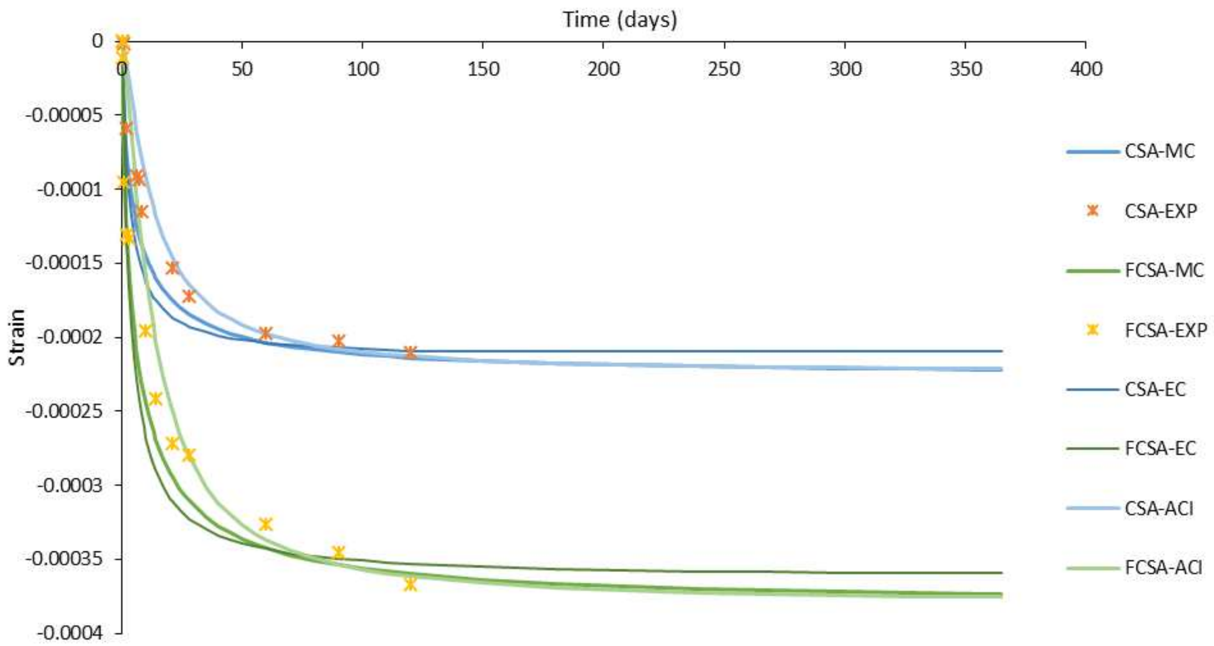

Figure 5. Experimental shrinkage of CSA and FCSA prisms and their predicted values based on MC, EC and ACI code

As the hydration reactions directly affect the strength development, these methods can be used to predict Shr_{Auto} for RSC and FRSC using the compressive strength of the sealed specimens, provided that *αbs* (a factor that is a function of cement type) is accurately calculated. The resulting shr_{Auto} for RSC and FRSC, following the MC approach and regression analysis is shown in Figure 6. The optimised *αbs* along with the compressive strength at 28 days of drying samples were used to predict the autogenous shrinkage component from the total shrinkage strain. FRSC has slightly higher autogenous shrinkage (4.79 %) than RSC prisms, likely due to its higher compressive strength.

The drying shrinkage is obtained by subtracting shr_{Auto} from the total strain. The MC was also used to predict the drying shrinkage by assigning suitable αds_1 and αds_2 for RSC and FRSC, see Figure 7. Although the ACI code does not consider separate components of shrinkage, it can also be used to predict the total shrinkage (Figure 7). The shrinkage parameters used to estimate shrinkage for each mix based on the different codes are listed in Table 3.

Table 3

Shrinkage parameters for various mixes

Mixes	Codes					
	MC		EC		ACI	
	αds_1	αds_2	αds_1	αds_2	P	α
CSA	0.1	0.012	0.29	0.11	108	1.32
FCSA	1.7	0.012	0.77	0.009	180	1.32

Mixes	Codes				
	MC			ACI	
	Shr_{Auto}	Shr_{Dry}		Shr_{Total}	
	αbs	αds_1	αds_2	P	α
RSC	17900	7	0.004	1320	1.65
FRSC	16780	5	0.004	1260	1.63

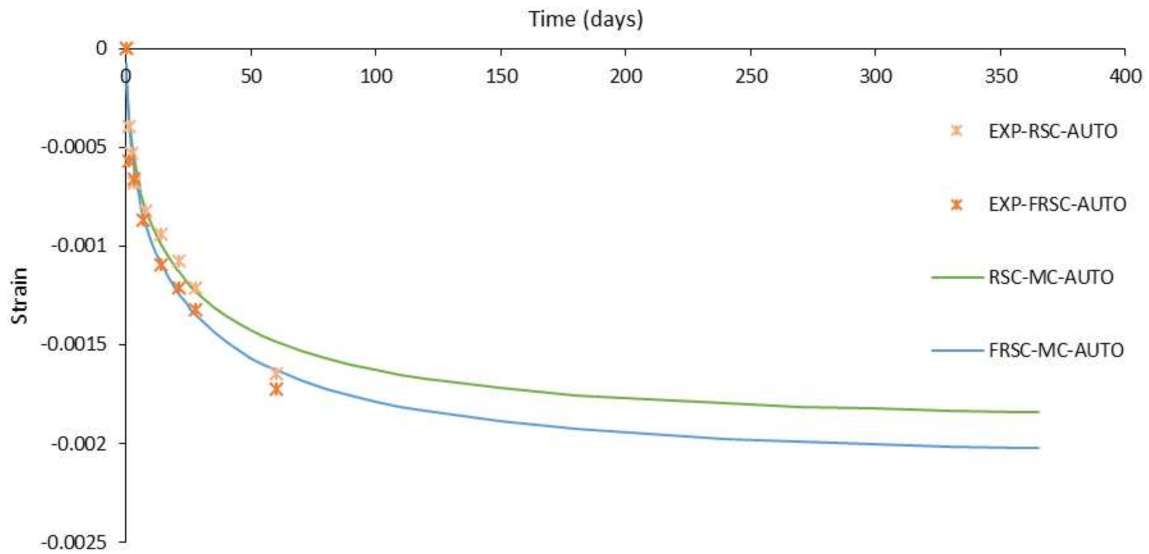

Figure 6. Experimental and predicted MC autogenous shrinkage of RSC and FRSC

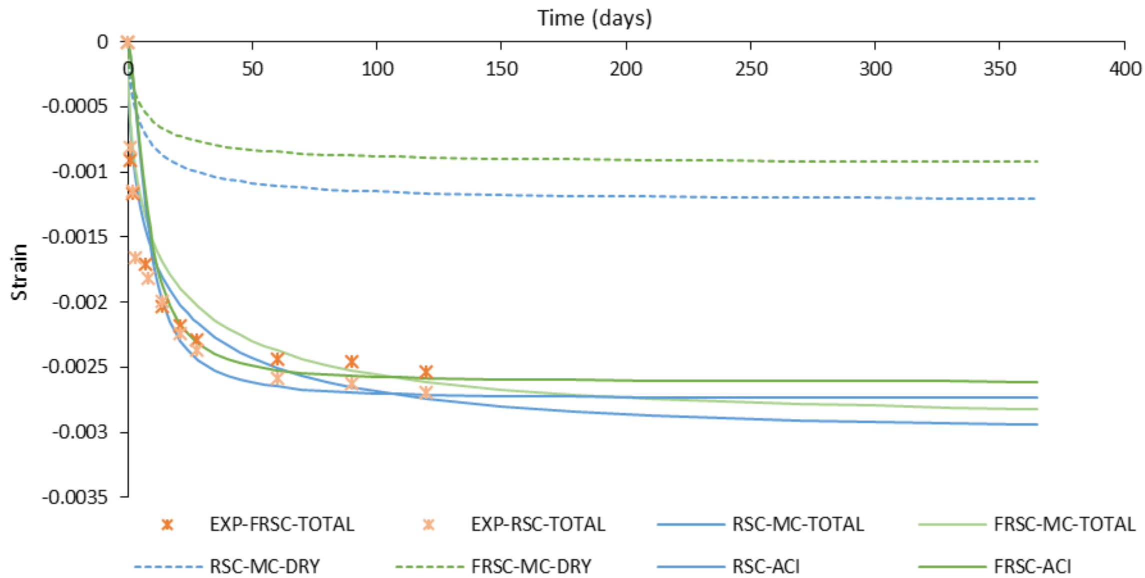

Figure 7. Experimental and predicted total and drying shrinkage of RSC and FRSC

It is interesting to note that the drying shrinkage of FRSC prisms seems to be smaller than RSC by around 12.6 % at the age of 365 days. This may be due to the fibre restraining effect. However, it should be noted that there is no consensus in the literature about the role of fibres on the free shrinkage strain.

4.3. Relationship between water loss and shrinkage

During the period of shrinkage monitoring, the weight of the prisms was recorded periodically. Figure 8 shows the relationship between water loss percent (W) and shrinkage for CSA and FCSA and RSC and FRSC respectively. It is clear that all mixes have a linear relationship between shrinkage and water content loss with strong correlations, although, as expected, with different multipliers.

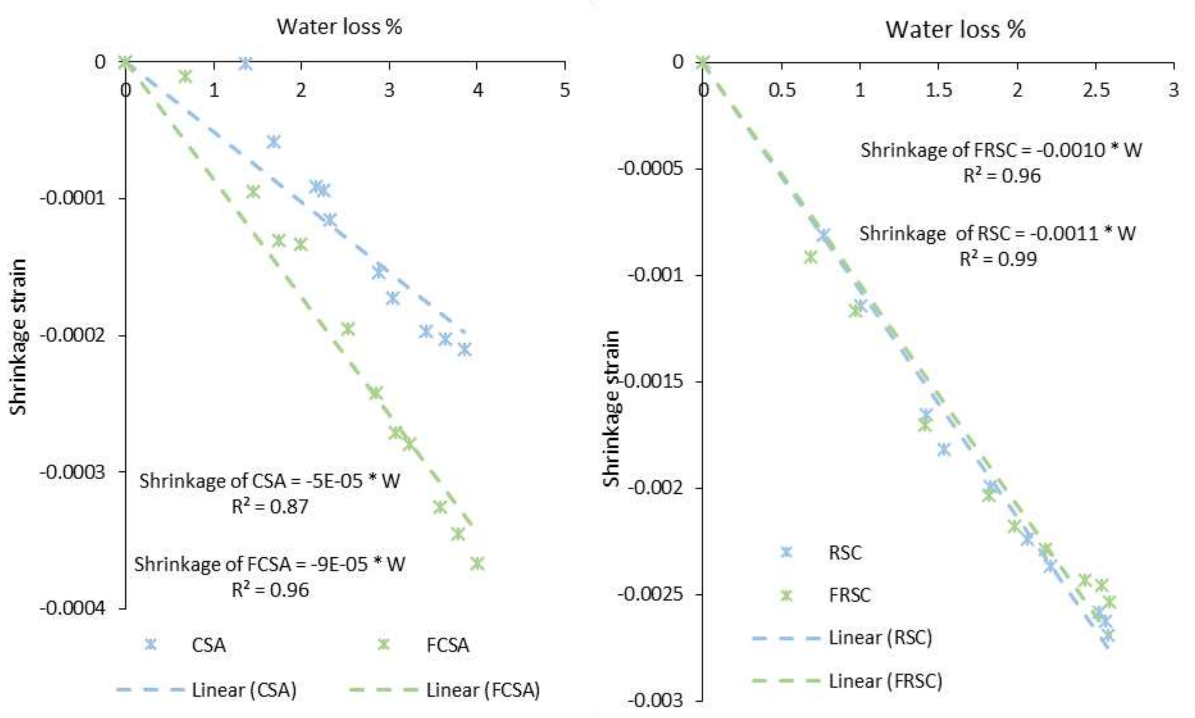

Figure 8. Experimental shrinkage versus measured water loss percent for: (a) CSA and FCSA; (b) RSC and FRSC prisms

Such linearity was also reported in [37] for concrete reinforced with post-consumer recycled steel fibres. In general, CSA and FCSA have more water loss than RSC and FRSC as they have higher initial water content (w/c = 0.4, 0.41 for CSA and FCSA respectively). The relationship also clearly highlights the effect of cement type on the shrinkage behaviour of the mixes. For example, for a 2.5 % water loss, the equivalent shrinkage for the mixes is 0.000125, 0.000225, 0.00275 and 0.0025 for CSA, FCSA, RSC and FRSC respectively. The water loss is also plotted against the calculated drying shrinkage for

RSC and FRSC specimens (Figure 9). This relationship is essential when introducing shrinkage in FE modeling through the hygral contraction coefficient

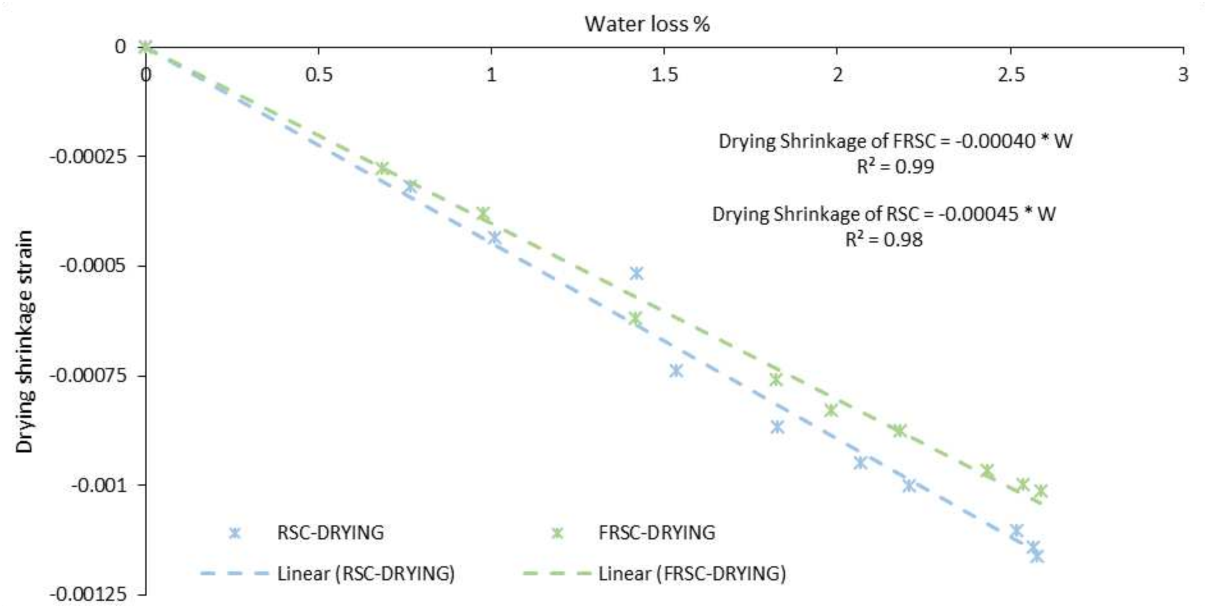

Figure 9. Calculated drying shrinkage versus measured water loss percent for RSC and FRSC prisms

5. Numerical studies

5.1. Numerical analysis approach

Heat transfer analysis available in FE package Abaqus was used to model moisture diffusion during drying. For this analysis, two parameters are essential; moisture diffusion and surface factor. The MC uses an equation that relates moisture diffusivity to relative humidity. As from the measurements taken only the normalized moisture content can be determined, this parameter is adopted instead of relative humidity as shown in Equation **8**.

$$D(C_{norm}) = D_1(\alpha + \frac{1-\alpha}{1+\left(\frac{1-C_{norm}}{1-C_c}\right)^n}) \qquad \text{Equation } \mathbf{8}$$

Where:

D_1 is the max diffusion coefficient when C_{norm} equals 1.0 and the samples are fully saturated (D_1 = 1

$\times 10^{-8}/f_{ck}$, f_{ck} = characteristic concrete strength),

α represents the ratio D_0/D_1; D_0 is the minimum D, C_c is the normalised moisture concentration at $D(C_{norm}) = 0.5D_1$.

The MC suggested values of $\alpha = 0.05$, $C_c = 0.8$ and $n = 15$ were initially used to calculate the diffusion coefficient. The resultant $D(C_{norm})$ for each mix was then adopted in the heat transfer analysis. Diffusive heat transfer 20-node quadratic brick elements (DC3D20) were used for the thermal analysis. As in the experiments, drying was only permitted through the top surface, which was assigned a surface factor, and the other surfaces were considered sealed having no moisture interaction with the environment. At the beginning of the drying, the normalised moisture concentration was 100% and the ambient relative humidity was considered constant at 40%. Initial values of the parameters for model code model of $D(C_{norm})$ as well as surface factors were optimized (Table 4) to minimize the difference between numerical and experimental moisture profile of each mix.

To calculate shrinkage deformations, the thermal analysis was coupled with a structural analysis in which the thermal expansion is replaced by a hygral contraction coefficient. C3D20R element type was used for the structural analysis. The tensile and compressive material characteristics were obtained from the experimental results and inverse analysis studies; further details on the procedures used are given elsewhere [6]. To accurately predict the shrinkage history, the development of the material properties with time was incorporated into the structural analysis through the implementation of the user subroutine, USDFLD. This allows the use of solution-dependent material properties and thus the user can define the field variables at a material point as a function of time [40]. The hygral coefficient was optimized to minimize the difference between measured experimental and FE predicted shrinkage strain.

5.2. Numerical results and discussion

5.2.1. Determination of moisture diffusivities and surface factor

The set of parameters implemented in MC equation (Equation **8**) [21] to determine the moisture diffusivity coefficient for each mix are listed in Table 4. The calculated moisture diffusivities for different mixes, as functions of normalized moisture content, C_{norm}, are shown in Figure 10. The results show that CSA has the highest moisture diffusion at the beginning of drying (34.8 mm^2/day) while FRSC has the lowest moisture diffusion (24.1 mm^2/day). The diffusivity is almost constant at the beginning of drying (for 1 - 0.77 moisture content), and then decreases sharply before stabilizing again. This behaviour is congruent with the mechanism of drying reported for conventional cementitious materials [12, 15, 16, 18]. For RSC and FRSC, to minimize the difference between measured and numerical moisture profiles, a slight change to MC approach was adopted. The slope of the tail of the moisture diffusivity against moisture content was reduced to zero (from C_{norm} = 0.66 downwards) instead of being almost constant as predicted by the MC equation.

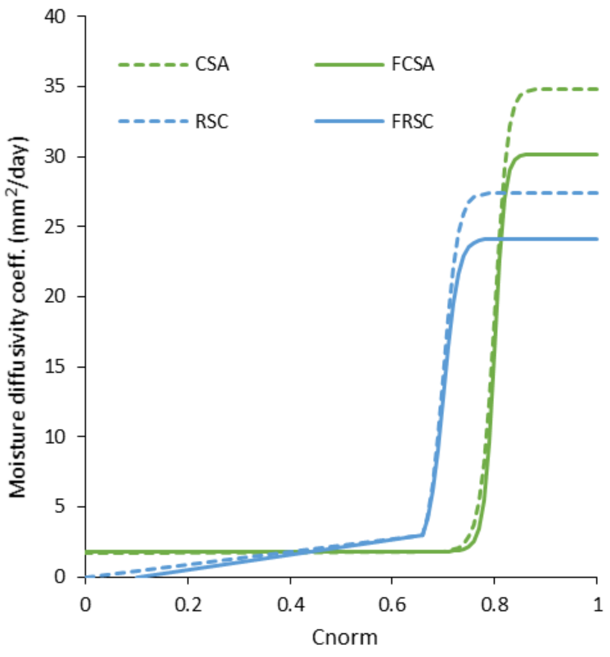

Figure 10. Moisture diffusivity versus normalized moisture content C_{norm}

A wide range of values is reported for moisture diffusivity (25.92 – 4665.6 mm^2/day) for well cured concrete specimens [29, 41, 42] and the results of this study seem to agree well with the lower bound of this range.

The back calculated surface factors for the tested mixes range from 4 – 6 mm/day. In addition, it was found that this factor only affects the moisture profiles near the drying surface and its effect diminishes quickly far from the top surface [18].

Table 4

Optimised parameters for MC equation and inverse analysis

Mix	*Optimised parameters of Equation 8*				*SF*	$\beta_{(C)}$
	D_1	α	C_c	*n*		
CSA	34.801	0.05	0.8	15	5	0.00038
FCSA	30.146	0.06	0.8	20	6	0.00065
RSC	27.399	0.035	0.7	20	4	0.0048
FRSC	24.139	0.05	0.7	20	4	0.0045

5.2.2. Determination of the hygral contraction coefficient

The hygral contraction coefficients for the mixes were back-calculated as functions of moisture content, *C*, using the free shrinkage test results. It was found that there is a strong linear relationship between shrinkage strain and moisture loss (Section 4.3), Equation **9**.

$$(\varepsilon_{sh})_M = \beta_{(C)} \times (C_0 - C) \qquad \text{Equation } \mathbf{9}$$

Where $(\varepsilon_{sh})_M$ is the free shrinkage strain, $\beta_{(C)}$ is the contraction coefficient and C_0 is the reference moisture content, 1.0. It should be noted that since both the total and drying shrinkage of RSC and FRSC show a linear relationship with water loss, the total shrinkage for samples of these mixes was modeled using a single hygral contraction coefficient. The calculated values of $\beta_{(C)}$ are listed in Table 4. As expected, mixes with calcium aluminate cement (CSA and FCSA) have much smaller contraction coefficient compared to the other mixes. However, for FCSA, $\beta_{(C)}$ is approximately 70% higher than that of CSA. This increase of shrinkage due to fibre addition is much higher than reported in literature. Nonetheless, those studies are only limited to Portland cement with/without pozzolanic additions. The value of $\beta_{(C)}$ for FRSC is slightly lower than that of RSC, possibly due to the restraining effect of the fibres at the large shrinkage strains developed.

5.2.3. Numerical moisture profiles: Results and Discussion

The numerical and experimental moisture profiles are compared in Figure 11. As it can be seen, the heat transfer analysis based on moisture diffusivities, calculated based on MC equation, predicts well the experimental moisture profiles with less than 5% difference.

5.2.4. Numerical shrinkage strain

The development of shrinkage strain with time, using parameters calculated in the previous sections, is compared to the experimental curves in Figure 12. As seen in Figure 12, the FE analysis satisfactorily represents the measured shrinkage, validating the factors adopted in the analysis.

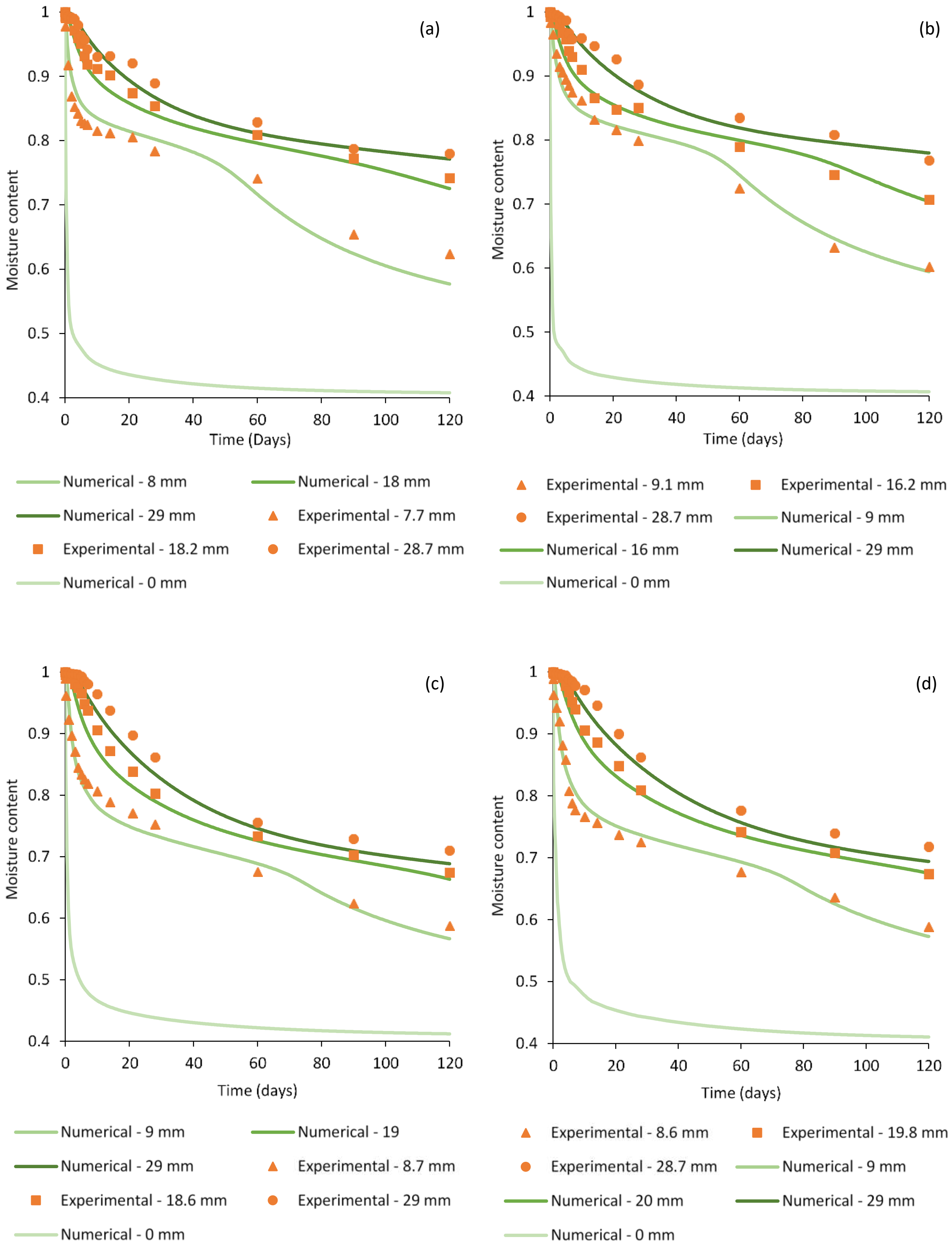

Figure 11. Numerical and experimental mositure profiles: (a) CSA; (b) FCSA; (c) RSC; (d) FRSC

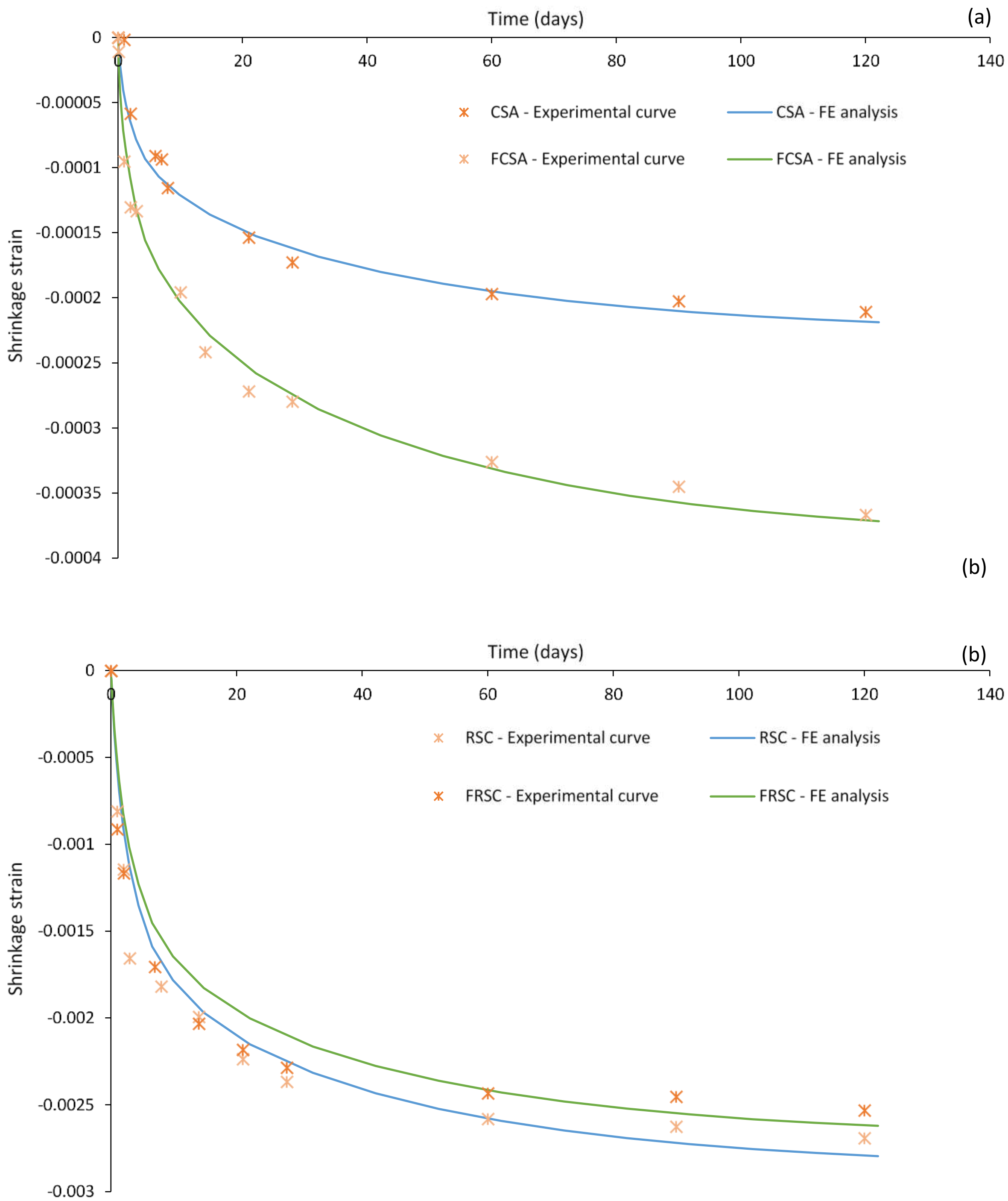

Figure 12. Numerical free shrinkage strain compared with experimental results: (a) CSA & FCSA; (b) RSC & FRSC

5.3. Comparison between numerical shrinkage and shrinkage predicted using MC, EC and ACI Code procedures

The parameters proposed for each code procedure to predict free shrinkage strain are used to obtain the free shrinkage of prisms of each mix with four different heights; 20, 30, 50 and 100 mm. The resulting curve for each mix, for a specific height, are compared with the FE predicted shrinkage (for that specific height) using the same parameters given in previous sections, Figs. 13-16.

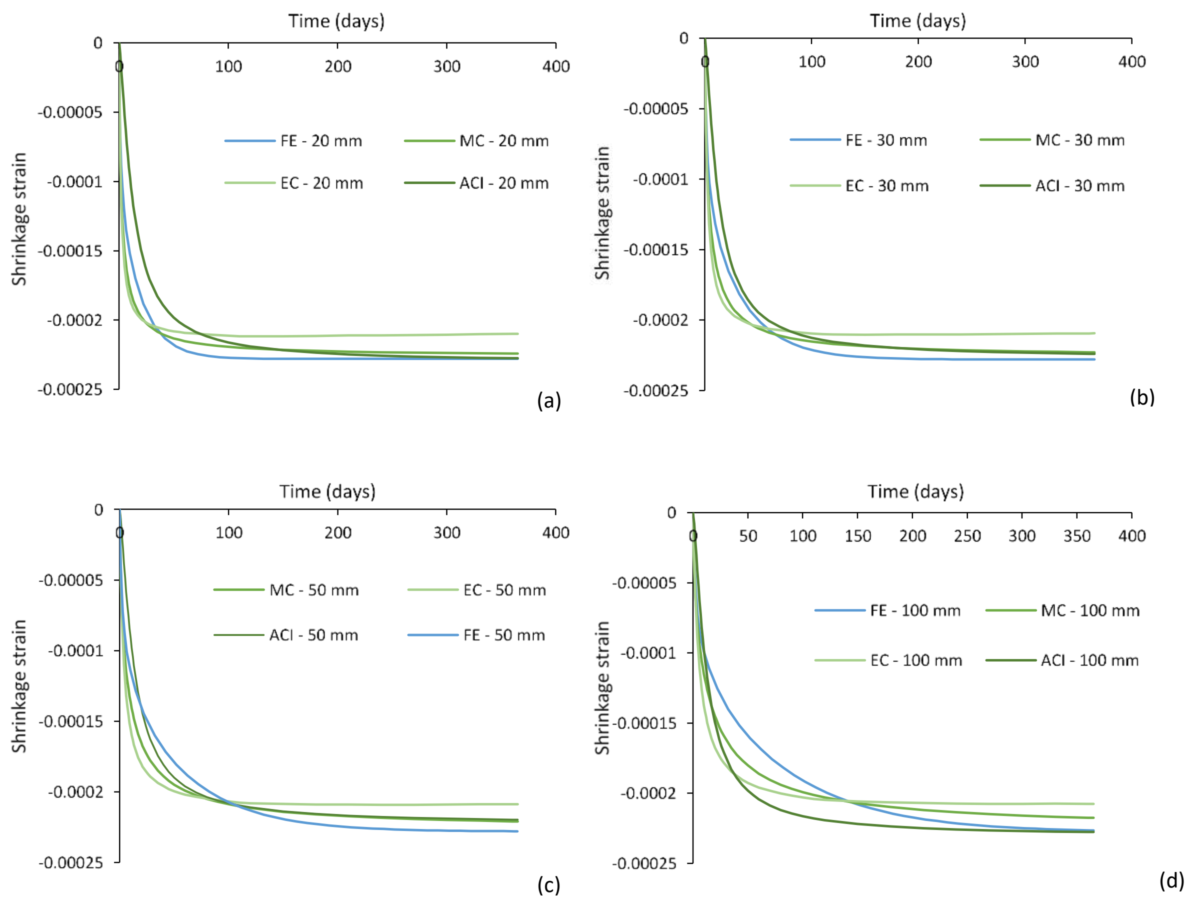

Figure 13. Numerical free shrinkage strain compared to shrinkage predicted using different codes for CSA prisms of heights: (a) 20 mm; (b) 30 mm; (c) 50 mm; (d) 100 mm

As seen in Figure 13 and Figure 14, the procedures are able to predict the shrinkage development of

CSA and FCSA samples, respectively, over time with reasonable accuracy, especially for thinner sections. The MC seems to offer the best estimate at both the beginning and the end of drying. However, EC appears to slightly overestimate the shrinkage at the beginning of drying while underestimates it towards the end of the testing period.

The estimated curves for total shrinkage development of RSC and FRSC over time against FE predicted curves are given in Figure 15 and Figure 16, respectively. It should be noted that EC was not used to predict shrinkage of RSC and FRSC mixes as it does not consider parameters for cement type in autogenous shrinkage prediction as it is the case in MC and, thus, was not used to model the shrinkage of RSC and FRSC mixes.

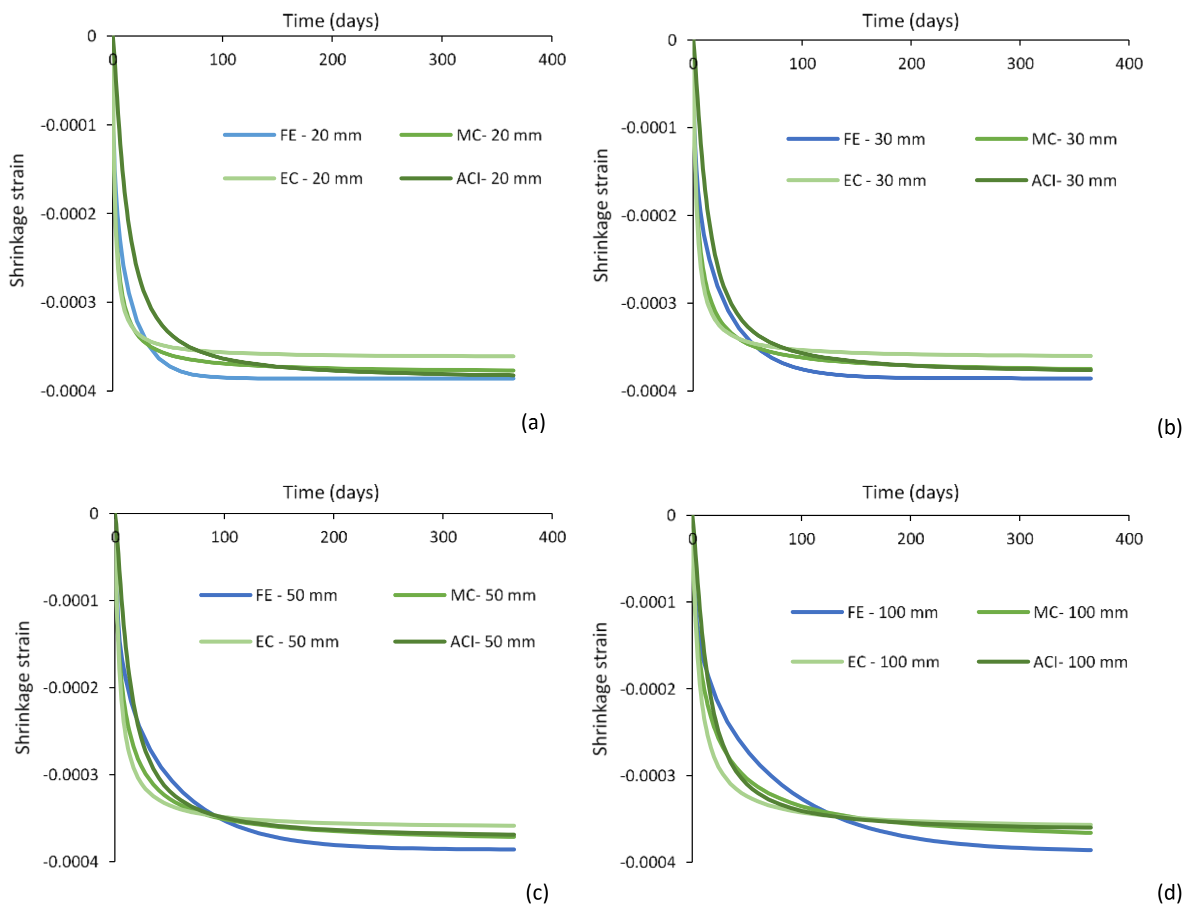

Figure 14. *Numerical free shrinkage strain compared to shrinkage predicted using different codes for FCSA prisms of depths: (a) 20 mm; (b) 30 mm; (c) 50 mm; (d) 100 mm*

As shown, for very thin sections, ACI offers slightly better predictions of shrinkage development with time compared to MC. At thicker sections, however, the MC seems to better capture the shrinkage history as ACI tends to overestimate the shrinkage development at the beginning of the testing and rather underestimates the shrinkage at later stages.

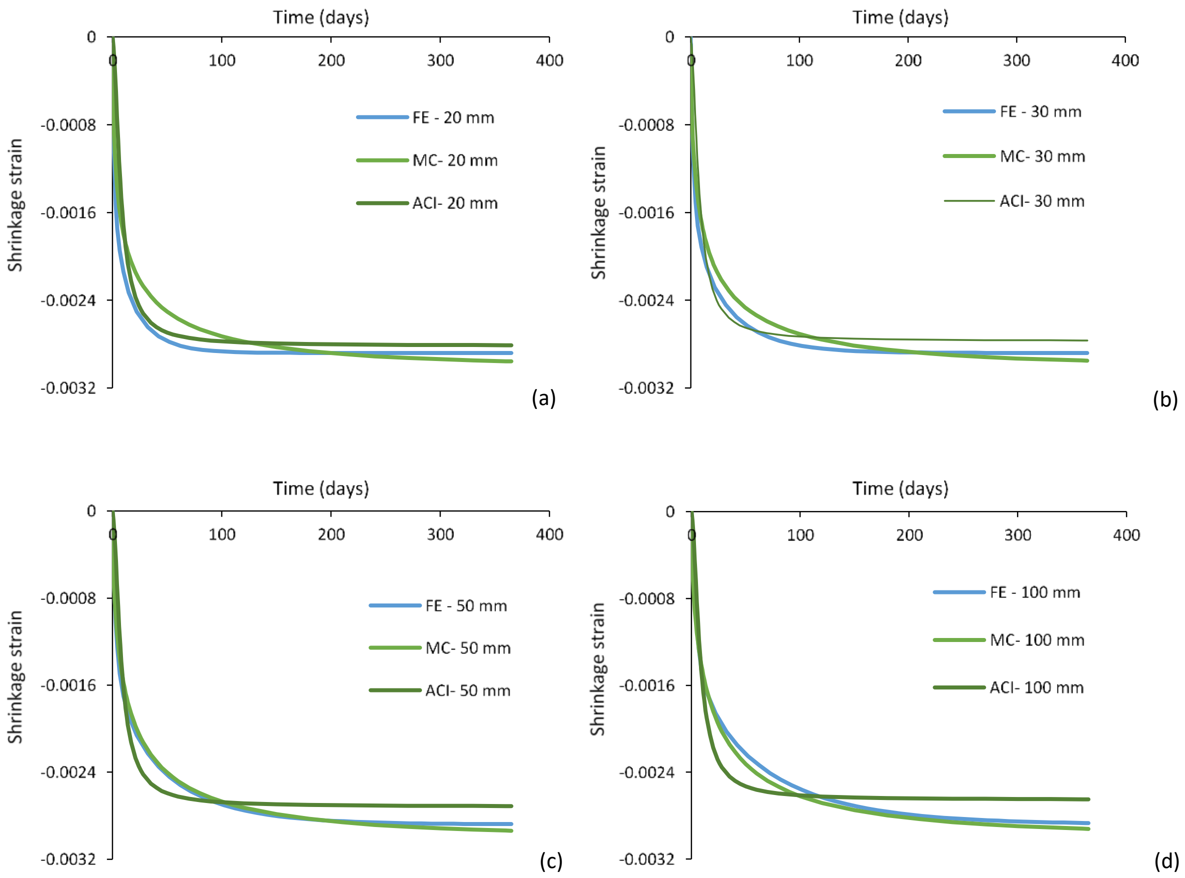

Figure 15. Numerical free shrinkage strain compared to shrinkage predicted using different codes for RSC prisms of heights: (a) 20 mm; (b) 30 mm; (c) 50 mm; (d) 100 mm

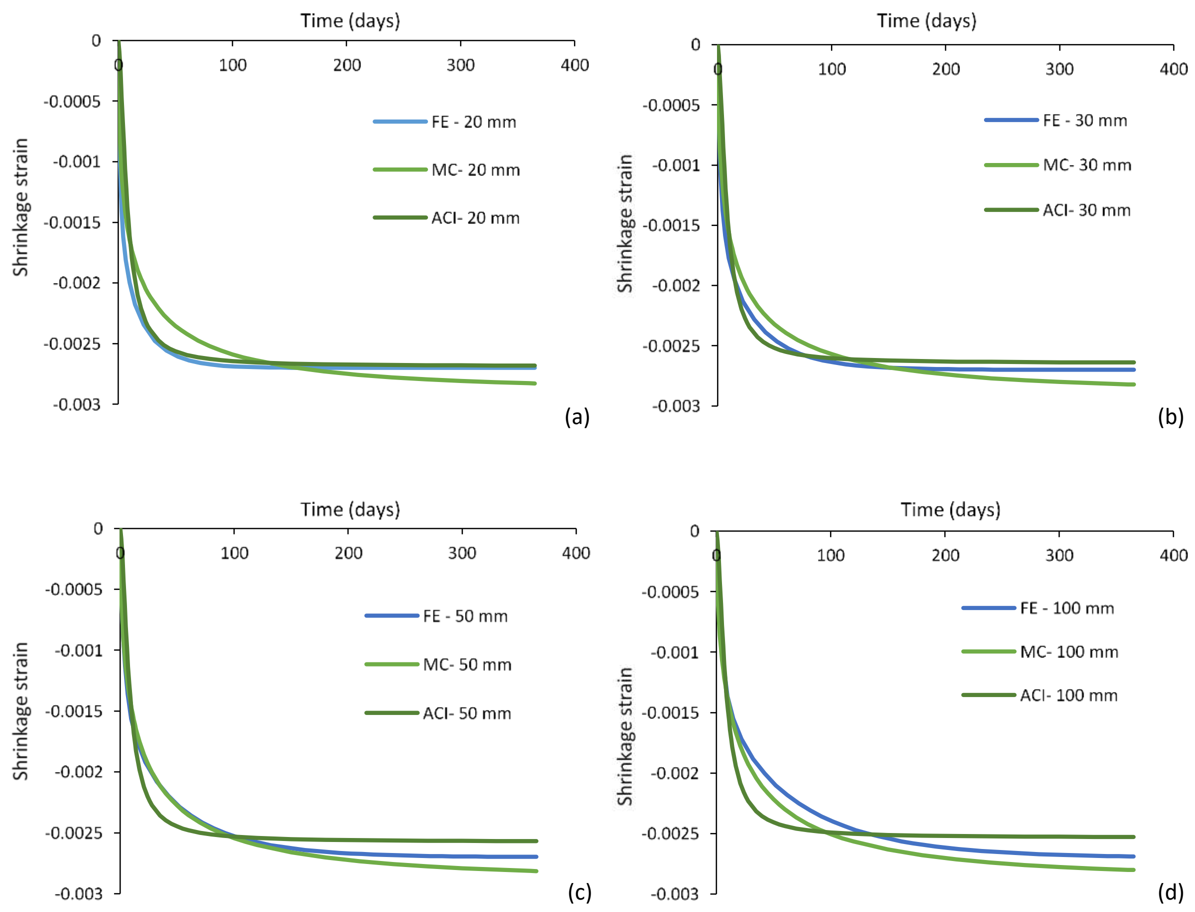

Figure 16. Numerical free shrinkage strain compared to shrinkage predicted using different codes for FRSC prisms of heights: (a) 20 mm; (b) 30 mm; (c) 50 mm; (d) 100 mm

6. Case studies

To assess the risk of cracking and/or delamination due to restrained shrinkage in repair layers prepared from the mixes developed in this study, the Silfwerbrand procedure [19] is followed. This requires knowing the free shrinkage of the overlay, the elastic modulus of the overlay layer and the substrate concrete as well as the tensile strength of the repair layer. The interface shear strength and the bond coefficient (K) should also be known.

To assess the risk of cracking and/or delamination, at one-year of age, the bonding conditions shown in Table 5 are considered. A layer with dimensions of 50*150*1000 mm is overlaid above an old concrete substrate with 200*150*1000 mm. The analysis is run twice for each mix; with and without creep in the overlay. When considering creep, the stresses were calculated by using the modulus of elasticity modified by creep coefficients. The creep coefficients were calculated based on the recommendations of MC 2010 [21]. As the substrate is already a few years old, it is considered conservative to neglect its creep deformations.

The calculated tensile stresses for CSA and FCSA overlaid prisms are shown in Fig. 17 while the shear stresses that develop at the interface are presented in Fig. 18 for different bond conditions. The effect of creep is also shown (curves labelled -c).

Table 5

Material properties used for the case studies

Layer type	E_c (GPa)	Tensile strength (MPa)	λL
Substrate	35	------	1
CSA	21.73	3.30	3
FCSA	28.00	4.00	10
RSC	20.56	3.02	30
FRSC	26.11	3.3	100

As shown in Figure 17 and Figure 18, neglecting creep leads to an overestimation of both tensile and shear stresses. When considering creep, for both CSA and FCSA overlays, the maximum tensile stress that develops at the interface is lower than the overlay tensile strength and thus it is predicted that cracking is unlikely to develop. However, for the strongest bond condition assumed (λL=100), high values of shear stresses develop with 6.11 MPa and 13.15 MPa for CSA and FSCA, respectively, at the edge of the composite prism, implying delamination if the shear strength at the interface is assumed to be similar to the tensile strength of concrete for well-prepared surfaces. For smaller λL, low shear stresses developed and thus the risk of delamination is lower (see Figure 18).

For RSC and FRSC overlays, cracking is predicted to occur for most bond conditions as the shrinkage strains are very high. The calculated shear stresses are also very high, indicating horizontal separation at the interface. However, in practice, as cracks develop, energy is released and shear stresses can drop.

The Silfwerbrand procedure does not clearly specify how to determine λL for different surface preparations and it is only useful in predicting cracking risk and, thus, the beneficial role of fibres cannot be quantified. Therefore, more experimental and analytical work is needed to understand how to accurately estimate λL and K (the bond constant) for different bond conditions. Such work can help provide better predictions of cracking and delamination risks, quantify the role of fibres in materials with high shrinkage values (over 2500 με) and residual strength higher than the cracking strength and determine whether or not fibres have a beneficial role in resisting/delaying delamination.

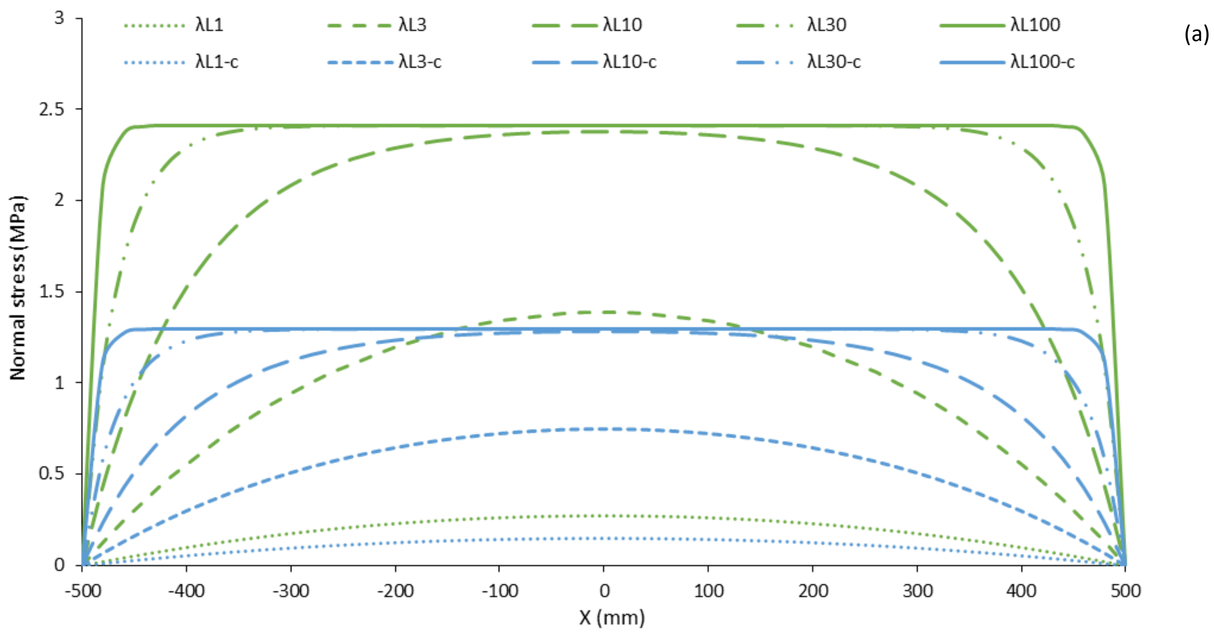

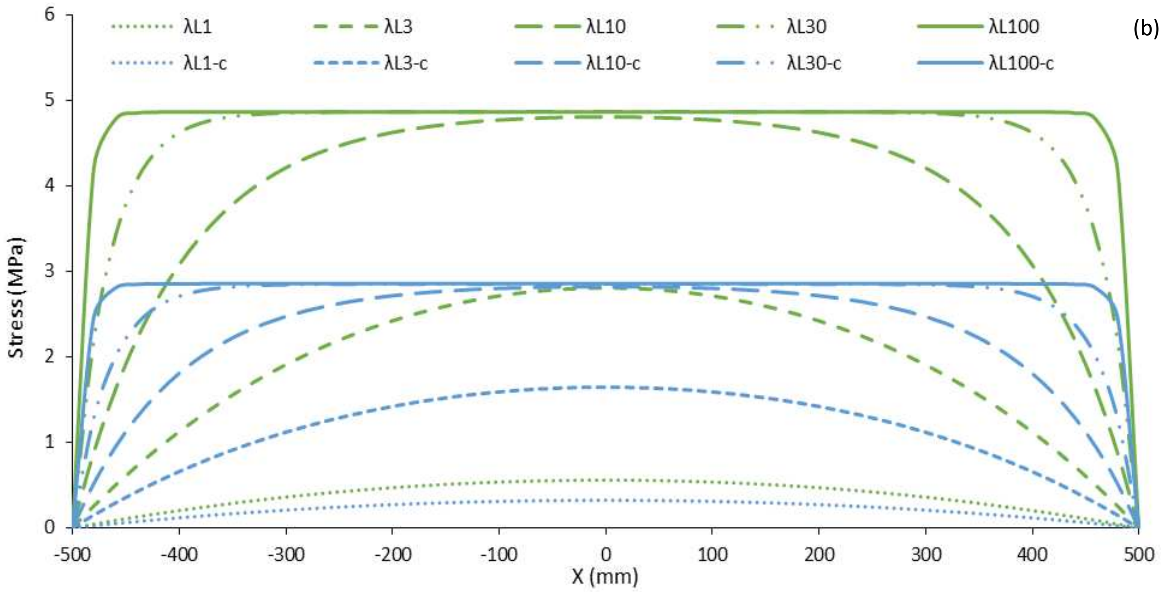

Figure 17. Normal stresses that develop at the interface between CSA overlay and substrate with and without creep for; (a) CSA overlay; (b) FCSA overlay

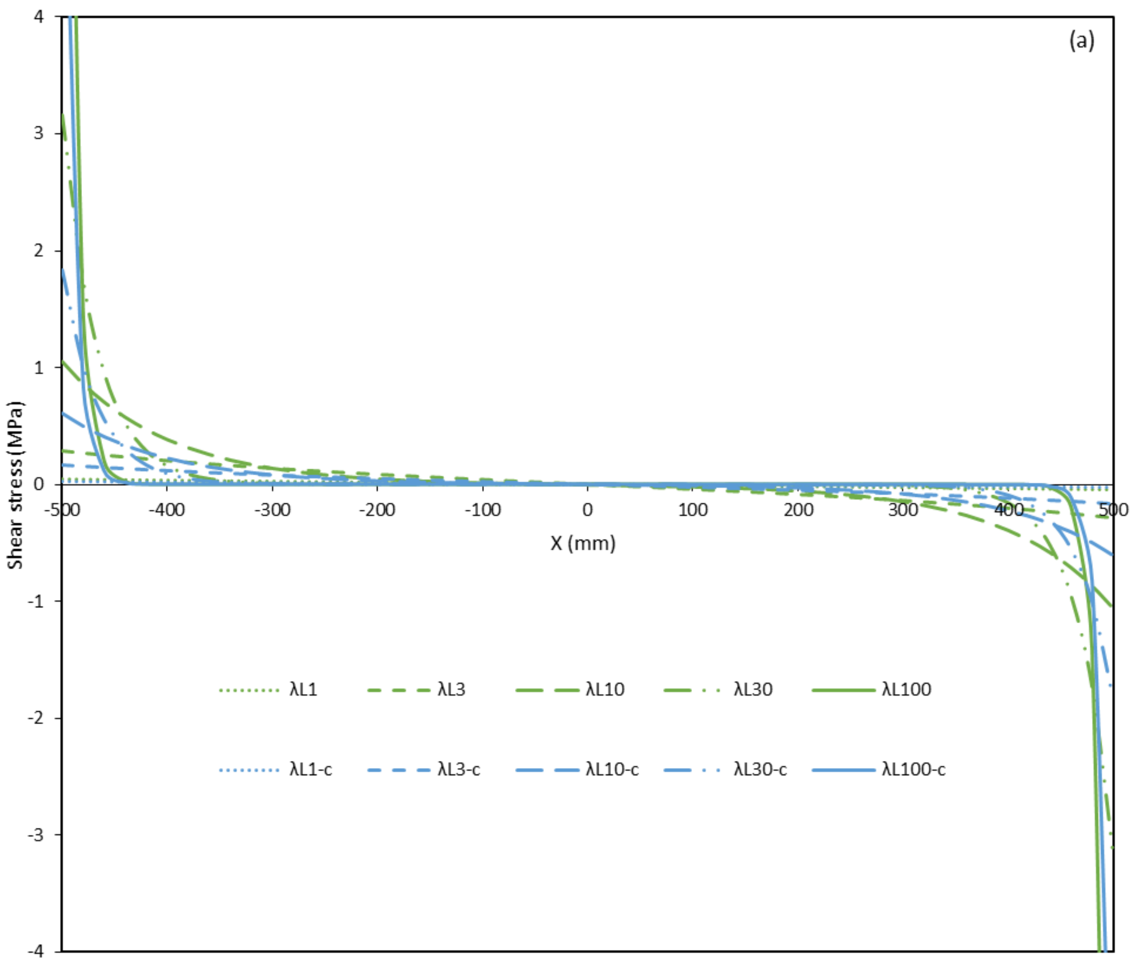

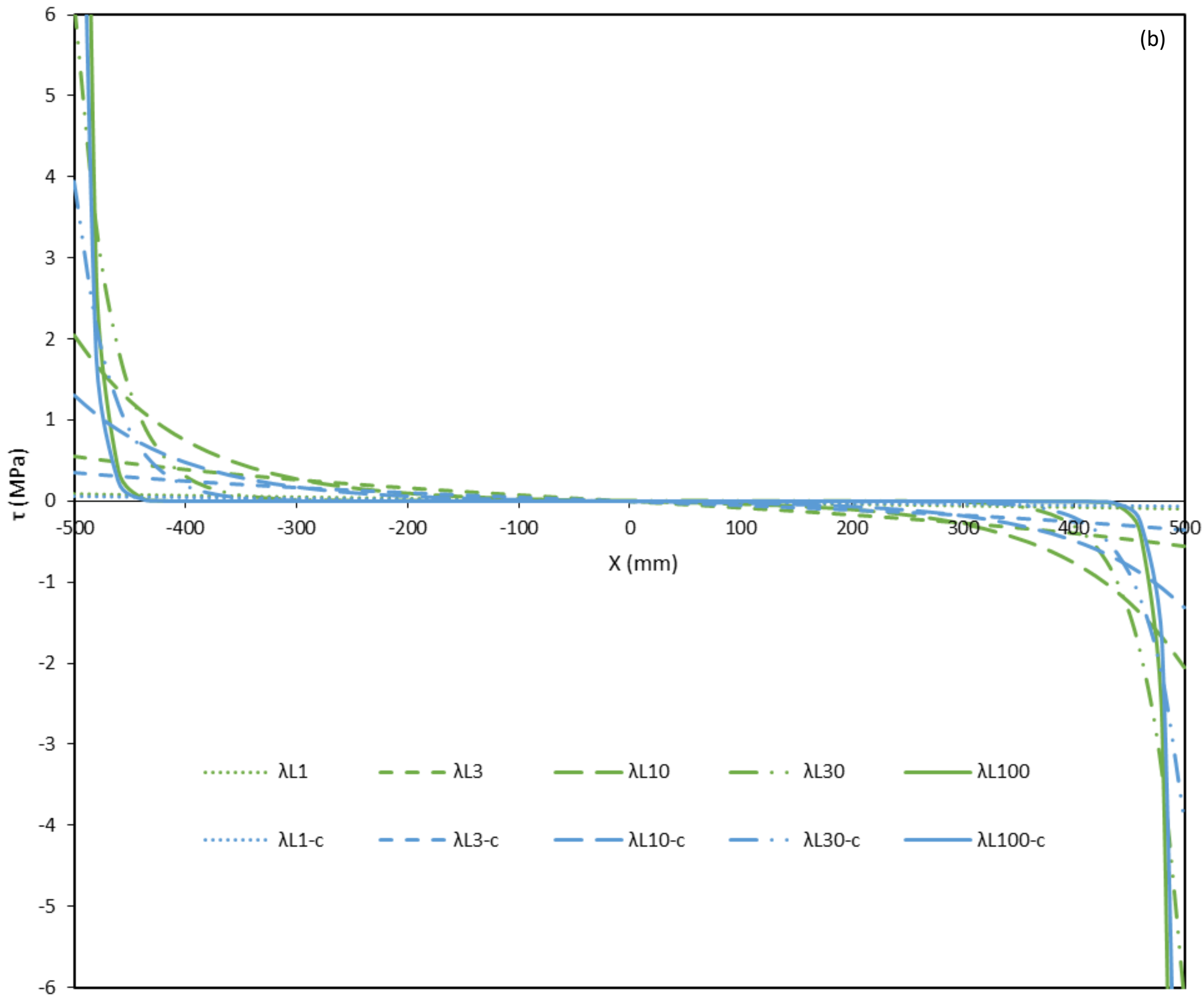

Figure 18. Shear stresses that develop at the interface between overlay and substrate with and without creep for; (a) CSA overlay; (b) FCSA overlay

Conclusions

This paper presents the main outcomes of a series of experimental and numerical studies on the time dependent transport properties of rapid hardening plain and fibre reinforced mortars for repair applications and on their shrinkage performance. Fibres are necessary to control crack widths in restrained conditions. The main findings of this study are:

- The fibre inclusion was confirmed not to have a major role on the moisture transport properties of rapid hardening mortar mixes, which allows the use of the MC equation, usually used to estimate the moisture diffusivity of plain concrete, to calculate their moisture diffusivities with good accuracy.

- Mixes with CSA cement showed much lower shrinkage strains (211 and 367 με) compared to mixes with RSC cement (2690 and 2532 με) at 120 days. Unlike CSA and FCSA, RSC and FRSC mixes showed considerable autogenous shrinkage which accounts for around 64 % and 71% of their total shrinkage at the age of 60 days.
- FE analyses were used in combination with experimental moisture distribution measurements to back calculate the moisture diffusivity of the tested mixes. It was found that the moisture diffusivities for mixes with rapid hardening cements are high at the beginning of drying (34.8 – 24.14 mm^2/day) and remain almost constant up to moisture contents of 85% - 75%, for different mixes, then sharply decreases upon further drying.
- There is a linear relationship between shrinkage and moisture loss for all the mixes with good correlation ratios.
- The hygral contraction coefficient, for each mix, were back calculated using inverse analysis for measured shrinkage strains. The coefficients range from 0.00038 to 0.0048 depending on the cement type and fibre inclusion.
- MC and ACI equations can be used to predict the shrinkage development with time provided appropriate coefficients for each cement type are used.
- Creep was found to play an important role in moderating tensile and shear stresses of the overlays.
- The Silfwerbrand procedure is used to determine normal and shear stresses in an overlay case study. Though the procedure is simple, it relies on parameters (λL and K) that are not easy to determine.

Acknowledgments

The authors acknowledge the financial support of the Higher Committee for Education Development in Iraq (HCED-Iraq) for the PhD studies of Hajir Al-musawi. The authors also thank Twincon Ltd for material supply and in-kind contributions.

References

[1] Beushausen, H., Alexander, M.G., (2006). Failure mechanisms and tensile relaxation of bonded concrete overlays subjected to differential shrinkage. *Cem*. *Concr*. *Res*. 36 (10), 1908-1914. Available at:

https://www.sciencedirect.com/science/article/pii/S0008884606001608.

[2] Scrivener, K., (2003). Calcium Aluminate Cement. In Newman, J., Advanced Concrete Technology. 2/1-2/29. Oxford: ButterworthHeinemann.

[3] Jewell, R., (2015). *Influence of Calcium Sulfoaluminate Cement on the Pullout Performance of Reinforcing Fibres: An Evaluation of the Micro-Mechanical Behavior*. PhD Thesis. University of Kentucky. Available at: http://uknowledge.uky.edu/ce_etds/27. [Accessed March 28, 2018].

[4] Swamy, R.N., Stavrides, H., (1979). Influence of fiber reinforcement on restrained shrinkage and cracking. In *Journal Proceedings*. *ACI J.* 76(3), 443-460.

[5] Graeff, A.G., Pilakoutas, K., Neocleous, K., Peres, M.V.N.N., (2012). Fatigue resistance and cracking mechanism of concrete pavements reinforced with recycled steel fibres recovered from post-consumer tyres. *Eng. Struct.* 45, 385–395. https://doi.org/10.1016/j.engstruct.2012.06.030.

[6] Al-musawi, H., Figueiredo, F., Bernal, S.A., Guadagnini, M., Pilakoutas, K., (2018). Performance of rapid hardening SFRC materials for repair applications. Accepted for publication.

[7] Hu, H., Papastergiou, P., Angelakopoulos, H., Guadagnini, M., Pilakoutas K., (2018). Mechanical properties of SFRC using blended recycled tyre steel cords and recycled tyre steel fibres, *Constr. Build. Mater*., 187, 553-564. Available at:

https://www.sciencedirect.com/science/article/pii/S0950061818318750?via%3Dihub.

[8] Banthia, N., Zanotti, C. and Sappakittipakorn, M., (2014). Sustainable fibre reinforced concrete for repair applications. *Constr. Build. Mater*., 67 (PART C), 405–412. Available at: http://dx.doi.org/10.1016/j.conbuildmat.2013.12.073.

[9] Xin, D., Zollinger, D.G., Allen, G.D., (1995). An approach to determine diffusivity in hardening concrete based on measured humidity profiles. *Adv*. *Cem*. *Based Mater*., 2(4), 138–144. Available at:

https://www.sciencedirect.com/science/article/pii/1065735595900144.

[10] Bazant, Z.P., Najjar L.J., (1972). Nonlinear water diffusion in non-saturated concrete. *Mater*. *Struct*., 5, 3–20. Available at:

https://link.springer.com/article/10.1007%2FBF02479073.

[11] Sakata, K., (1983). A study on moisture diffusion in drying and drying shrinkage of concrete. *Cem*. *Concr*. *Res*., 13(2), 216–224. Available at:

https://www.sciencedirect.com/science/article/pii/0008884683901047.

[12] Selih, J., Sousa, A.C.M., Bremner, T.W., (1996). Moisture transport in initially saturated concrete during drying. Transp. Porous Media, 24, 81–106. Available at:

https://link.springer.com/article/10.1007%2FBF00175604.

[13] Ayano, T., Wittmann, F.H., (2002). Drying moisture distribution, and shrinkage of cement-based materials. *Mater*. *Struct*., 35, 134–140. Available at:

https://link.springer.com/article/10.1007%2FBF02533581.

[14] Shekarchi, M., Bonakdar, A., Bakhshi, M., Mirdamadi, A., Mobasher, B., (2010). Transport properties in metakaolin blended concrete. *Constr*. *Build*. *Mater*., 24 (11), 2217-2223. Available at: https://www.sciencedirect.com/science/article/pii/S0950061810001558.

[15] Bakhshi, M., Mobasher, B., (2011). Experimental observations of early-age drying of Portland cement paste under low-pressure conditions. *Cem*. *Concr*. *Compos*., 33(4), 474-484. Available at: https://www.sciencedirect.com/science/article/pii/S0958946511000229.

[16] Bakhshi, M., Mobasher, B., Soranakom, C., (2012). Moisture loss characteristics of cement-based materials under earlyage drying and shrinkage conditions. *Constr*. *Build*. *Mater*., 30, 413–425. Available at: https://www.sciencedirect.com/science/article/pii/S0950061811006453?via%3Dihub.

[17] Bakhshi, M., Mobasher, B. and Zenouzi, M., (2012). Model for early-age rate of evaporation of cement-based materials. *J*. *Eng*. *Mech*., 138 (11), 1372-1380.

[18] Jafarifar, N., (2012). *Shrinkage behaviour of steel-fibre-reinforced-concrete pavements*. PhD thesis. University of Sheffield. Available at: http://etheses.whiterose.ac.uk/7475/.

[19] Silfwerbrand, J., (1997). Stresses and strains in composite concrete beams subjected to differential shrinkage. *ACI Struct*. *J*., 94(4), 347-353.

[20] CEN, (2004). Eurocode 2: Design of concrete structures, Part 1-1: General rules and rules for buildings. European Committee for Standardization. Brussels, Belgium.

[21] F.I. du Béton, (2013). Fib Model Code for Concrete Structures 2010, Wilhelm Ernst & Sohn, Berlin, Germany.

[22] ACI, (2008). ACI 209.2R-08: guide for modeling and calculating shrinkage and creep in hardened concrete. American Concrete Institute, Farmington Hills.

[23] Azenha, M., Maekawa, K., Ishida, T. and Faria, R., (2007). Drying induced moisture losses from mortar to the environment. Part I: experimental research. *Mater*. *Struct*., 40(8), 801-811. Available at: https://link.springer.com/article/10.1617/s11527-007-9244-y.

[24] Lura, P., Pease, B., Mazzotta, G.B., Rajabipour, F. and Weiss, J., (2007). Influence of shrinkage-reducing admixtures on development of plastic shrinkage cracks. *ACI Mater*. *J*., 104(2), 187-194.

[25] Hall, C., Hoff, W.D. and Nixon, M.R., (1984). Water movement in porous building materials—VI. Evaporation and drying in brick and block materials. *Build*. *Environ*., 19(1), 13-20.

[26] Hall, C. and Hoff, W.D., (2002). Water transport in brick, stone and concrete. New York: Taylor & Francis.

[27] Vu T.H., (2006). *Influence of pore size distribution on drying behaviour of porous media by a continuous model*. MSc Dissertation. Germany: Otto-von-Guericke-Universität Magdeburg.

[28] Huang, H., Garcia, R., Guadagnini, M. and Pilakoutas, K., (2017). Effect of section geometry on development of shrinkage-induced deformations in box girder bridges. *Mater*. *Struct*., 50:222. Available at: https://link.springer.com/article/10.1617/s11527-017-1090-y.

[29] Baluch, M.H., Rahman, M.K., Al-Gadhib, A.H., Raza, A. and Zafar, S., (2006). Crack minimization model for hot weather concreting. *Arabian J*. *Sci*. *Eng*., 31(1C), 77-91.

[30] BS EN 13892-2, (2002). Methods of test for screed materials — Part 2: Determination of flexural and compressive strength.

[31] JSCE-SF4, (1984). Standard for Flexural Strength and Flexural Toughness, Method of Tests for Steel Fiber Reinforced Concrete, Concrete library of JSCE, Japan Concrete Institute (JCI), Japan.

[32] ASTM C191, (2013). Standard Test Method for Time of Setting of Hydraulic Cement by Vicat Needle. *ASTM International*, (May), 1-8.

[33] ASTM C 157, (2008). Test method for length change of hardened hydraulic cement mortar and concrete. *ASTM International*.

[34] Pera, J., and Ambroise, J., (2004). New applications of calcium sulfoaluminate cement. *Cem*. *Concr*. *Res*., 34(4), 671-676.

[35] Winnefeld, F., and Lothenbach, B., (2010). Hydration of calcium sulfoaluminate cements—experimental findings and thermodynamic modelling. *Cem*. *Concr*. *Res*., 40(8), 1239-1247.

[36] Scrivener, K. (2003). Calcium Aluminate Cement. In Newman, J. and Choo, B.S., *Advanced Concrete Technology*. 2/1-2/29. Oxford: Butterworth-Heinemann.

[37] Al-Kamyani, Z., Guadagnini M., and Pilakoutas, K., (2018). Predicting shrinkage induced curvature in plain and reinforced concrete. *Eng*. *Struct*. *J*., 176, 468-480. Available at:

https://www.sciencedirect.com/science/article/pii/S014102961831023X.

[38] Neville, A.M., (1995). *Properties of concrete* (4th ed.). London: Longman.

[39] Wu, L., Farzadnia, N., Shi, C., Zhang, Z. and Wang, H., (2017). Autogenous shrinkage of high performance concrete: A review. *Constr*. *Build*. *Mater*., 149, 62-75.

[40] ABAQUS 2017 Documentation.

[41] Bažant, Z.P. and Najjar, L.J., (1971). Drying of concrete as a nonlinear diffusion problem. *Cem*. *Concr*. *Res*., 1(5), 461-473.

[42] Kim, J.K. and Lee, C.S., (1999). Moisture diffusion of concrete considering self-desiccation at early ages. *Cem*. *Concr*. *Res*., 29(12), 1921-1927.